

Towing tank PIV measurement system and data and uncertainty assessment for DTMB Model 5512

L. Gui, J. Longo, and F. Stern
Iowa Institute of Hydraulic Research
The University of Iowa, Iowa City, IA 52242, USA

Abstract A towed PIV system designed by DANTEC Measurement Technology for the Iowa Institute of Hydraulic Research towing tank is commissioned by measuring the mean velocity and Reynolds stresses at the nominal-wake plane of a model-scale ship. The mean velocities are compared with previous 5-hole pitot probe data. Uncertainty assessment following standard procedures is used to quantify the comparisons and reach conclusions regarding the quality of the data.

1

Introduction

Experimental fluid dynamics (EFD) research at the Iowa Institute of Hydraulic Research (IIHR) towing tank is conducted for understanding physics of ship hydrodynamics, supporting development of Reynolds-averaged Navier Stokes (RANS) simulation methods, and contributing to the database for model-scale surface ship resistance and propulsion. Recent evaluation of the database (Stern et al., 1998) indicates that validation data for turbulence and unsteady flow are especially lacking.

Validation of RANS codes for steady flow requires dense mappings of the time mean and root-mean-square (RMS) flow at multiple crossplanes. Recent examples for time mean flow include Toda et al. (1992) and Longo and Stern (1996). 5-hole pitot probes are traditionally used for measuring time mean velocities. Because of the intrusive nature of the probe, the measurements in areas of high velocity gradient and turbulence contain biases not accounted for in usual calibration procedures. Additionally, this type of measurement, i.e., water-transmission of pressures through a multi-hole probe coupled with differential pressure transducers is not capable of measuring Reynolds stresses, which are required for understanding physics of turbulence-free surface interaction and development of turbulence models.

Laser-Doppler velocimetry (LDV) has been used in towing tanks for reducing probe disturbance effects and measuring mean velocities and Reynolds stresses (Fry and Kim, 1985; Hoekstra and Ligtelijn, 1991; Longo et al. 1998). These measurement systems require point-to-point techniques, which are time consuming and usually produce many data planes with coarse spacing or few planes with higher resolution.

In consideration of the above, the optical and large-field measurement technique, particle image velocimetry (PIV), is

an ideal choice for high spatial resolution and relatively fast mean velocity and Reynolds stress measurement in towing tanks. PIV was used in a towing tank by Dong et al. (1997) to study bow flow for a ship model. However, a stationary system was used, which is only capable of obtaining limited instantaneous PIV images in a carriage run. A stationary PIV system practicably precludes the ability to obtain mean velocity and Reynolds stress data, which are derived from hundreds of instantaneous snapshots of the flow. On the other hand, a towed PIV system enables acquisition of sufficient image pairs for evaluation of mean velocities and Reynolds stresses by sampling the same area many times in succession. IIHR has obtained a towed PIV system designed by DANTEC Measurement Technology, which was commissioned by measuring the mean velocities and Reynolds stresses at the nominal-wake plane of David Taylor Model Basin (DTMB) model 5512. The mean velocities are compared with previous 5-hole pitot probe data. Uncertainty assessment following standard procedures is used to quantify the comparisons and reach conclusions on the quality of the data. It is the first application of a towed PIV system for towing tanks.

The work is also part of an international collaborative project between IIHR, Istituto Nazionale per Studi ed Esperienze di Architettura Navale (INSEAN), and David Taylor Model Basin (DTMB) on EFD/CFD and uncertainty assessment for a combatant geometry. The present work has three goals: (1) test the overall effectiveness of the PIV system through cross-validation of the 5-hole pitot and PIV data; (2) measure the turbulent flow field; and (3) complete a detailed uncertainty assessment of the results.

2

The IIHR towed PIV measurement system

The IIHR towing tank is 100 m long and 3.05 m wide and deep and equipped with a drive carriage and trailers on which the PIV system is installed. The DANTEC PIV hardware and software are integrated into a single measurement system. The PIV hardware components (hydrodynamic strut, Nd:Yag laser, light-guiding arm, light-sheet optics, digital camera) are built around a massive 2D, computer-controlled traversing system capable of automated movement along the transverse (y) and vertical (z) axes. Movement of the strut along the axis of the tank (x) is done manually. The hydrodynamic strut is pressurized, partly submerged, and contains a 20 mJ, dual cavity Nd:Yag laser and light-guiding

arm for steering the 532 nm beams into the light-sheet optical package which resides in a submerged, streamlined torpedo. The digital camera is a 1K×1K (1008×1018 pixels) cross-correlation camera fitted with a f/1.4 50 mm lens that views the light sheet from a distance of 50 cm through a 90° mirror. The camera is also housed in a submerged, streamlined torpedo. The two torpedoes are fixed to the strut in a way such that the light sheet is orthogonal to the axis of the camera. The system can be configured to measure in three planes of interest: vertical (xz); horizontal (xy); and crossplane (yz). Although the later configuration was shown to suffer from parallax errors, more testing is needed, therefore, the yz configuration is not used in this study. With the 50 mm lens, the measurement area is 7.47×7.54 cm. Silver-coated hollow glass spheres with a density of 1300 kg/m³ and an average diameter of 15 μm are used as seed particles. These particles have demonstrated very good light-reflectance for PIV image capture and adequate suspension capability. Additionally, the particles are capable of following sinusoidal motions with frequencies up to 1375 Hz (Dring, 1982). Synchronization of the laser and camera, image processing, and acquisition of towing carriage speed (U_c) are done with the Dantec PIV 2000 processor. Data acquisition and parameter settings are enabled with Dantec FlowMap v.3.0 software from an IBM compatible PC. Results in the form of vector maps are displayed virtually in real-time at a data rate of 7.5 Hz.

3 Test design

The geometry of interest is the 3.048 m DTMB model 5512. A right-handed Cartesian coordinate system is used with the origin at the intersection of the undisturbed free surface and forward perpendicular (FP, x=0) of the model. The x, y, z axes are directed downstream, transversely to starboard, and upward, respectively. The model is towed in the fixed condition at the dynamic sunk and trimmed condition corresponding to Fr=0.28. The carriage speed is U_c=1.53 m/s and the Reynolds number (Re)=5.2×10⁶. At this towing speed, a 30 second window of data acquisition is available which produces roughly 200 vector maps. The nominal-wake plane (x=0.935) is the region of interest and the variables of interest (U, V, W, \overline{uu} , \overline{vv} , \overline{ww} , \overline{uv} , \overline{uw}) are mapped on the port side of the hull by taking measurements in the xz- and xy-configurations and reconstructing the yz-plane through post processing procedures. The final measurement area at x=0.935 is 14×15 cm and contains 18 z-cuts from the xy-configuration and 20 y-cuts from the xz-configuration. In each configuration, two or three locations of the camera and lightsheet are required to cover the total measurement area and provide adequate overlap between individual measurement areas.

PIV image pairs are taken with a time interval of Δt=490 μs so that the maximal particle image displacement in the image pairs is about 10 pixels. A 32×32-pixel interrogation window is chosen for evaluating the image pairs with a cross-correlation algorithm. A window offset of 8 pixels in the main flow direction is used for reducing the evaluation

errors. A window function Westerweel (1997) and Gui et al. (1999) is used for further improvement of the evaluation. An overlap of 50% is selected for the evaluation in order to get more detailed information about the turbulence structures. For every test case, about N=1200 raw vector maps are recorded. A 3-D median filter (the third dimension is the time sequence) is used for detecting and removing spurious vectors. The final results are produced by a statistical analysis of the valid velocity vectors and nondimensionalization with U_c.

4 Uncertainty assessment

The uncertainty assessment of the measurement results follows the AIAA Standard (1995). The 95% confidence large-sample approach recommended by the standard is derived and explained in detail by Coleman and Steele (1995). A summary of uncertainty assessment results for the PIV and previous 5-hole pitot probe results are provided in Tables 1 and 2.

4.1 Bias limits of the mean velocity components

For convenience, the mean velocity component is defined as C_k, where k equals 1, 2, 3 for the coordinates x, y, z, respectively. The instantaneous velocity component C_{k,i} (one of measurement samples with total number N) is determined with

$$C_{k,i} = \frac{L_{obj} \cdot S_{k,i}}{L_{img} \cdot \Delta t \cdot U_c} \quad \text{for } k = 1, 2, 3; i = 1, 2, \dots, N \quad (1)$$

where L_{obj} is the width of the camera view in the object plane, L_{img} is the width of the digital image, and S_{k,i} is the component of the particle image displacement obtained by evaluating the digital PIV recording. The mean velocity component C_k can be determined with the mean particle displacement component S_k as

$$C_k = \frac{L_{obj}}{L_{img} \cdot \Delta t \cdot U_c} \cdot \frac{1}{N} \sum_{i=1}^N S_{k,i} = \frac{L_{obj}}{L_{img} \cdot \Delta t \cdot U_c} S_k \quad (2)$$

The measured mean-velocity components are spatially-dependent, therefore, C_k can be written as

$$C_k = C_k(L_{obj}, L_{img}, \Delta t, U_c, S_k, x, y, z) \quad (3)$$

The bias limit of C_k is determined with a root-sum-square (RSS) of the elementary bias limits

$$B_{C_k}^2 = \theta_{L_{obj}}^2 B_{L_{obj}}^2 + \theta_{L_{img}}^2 B_{L_{img}}^2 + \theta_{\Delta t}^2 B_{\Delta t}^2 + \theta_{U_c}^2 B_{U_c}^2 + \theta_{S_k}^2 B_{S_k}^2 + \theta_x^2 B_x^2 + \theta_y^2 B_y^2 + \theta_z^2 B_z^2 \quad (4)$$

where the sensitivity coefficients are defined as

$$\theta_X = \frac{\partial C_k}{\partial X}, \quad X = (L_{obj}, L_{img}, \Delta t, U_c, S_k, x, y, z) \quad (5)$$

4.2

Bias limits of the Reynolds stresses

Again for convenience, the normal stress is defined as $\overline{c_k c_k}$ and the shear stress as $\overline{c_m c_n}$ where $m=1,2,3; n=1,2,3; m \neq n$. The bias limits of the normal and shear stresses are derived with statistical analyses. The measured instantaneous velocity $C_{k,i}$ is the sum of the true value C_k^o , the bias error $\beta_{k,i}$, and the random error $\epsilon_{k,i}$

$$C_{k,i} = C_k^o + \beta_{k,i} + \epsilon_{k,i} \quad (6)$$

The measured and true mean velocity component are defined as

$$C_k = \frac{1}{N} \sum_{i=1}^N C_{k,i}, \quad C_k^o = \frac{1}{N} \sum_{i=1}^N C_k^o \quad (7)$$

If N is large enough, the sum of the random errors can be neglected, and the bias error of the mean velocity component equals the mean of the instantaneous bias error

$$\beta_k = C_k - C_k^o \approx \frac{1}{N} \sum_{i=1}^N \beta_{k,i} \quad (8)$$

The mean bias error β_k can be shown to be a function of the true mean velocity component C_k^o . Therefore, a bias gradient can be defined as

$$\tau_k = \frac{d\beta_k}{dC_k^o} \quad (9)$$

The instantaneous bias error can approximately be determined by

$$\beta_{k,i} \approx \beta_k + \tau_k (C_{k,i}^o - C_k^o) \quad (10)$$

The measured and true normal stress are defined as

$$\overline{c_k c_k} = \frac{1}{N} \sum_{i=1}^N (C_{k,i} - C_k)^2, \quad \overline{c_k^o c_k^o} = \frac{1}{N} \sum_{i=1}^N (C_{k,i}^o - C_k^o)^2 \quad (11)$$

and are related by

$$\overline{c_k c_k} = (1 + \tau_k)^2 \overline{c_k^o c_k^o} + \frac{2(1 + \tau_k)}{N} \sum_{i=1}^N \epsilon_{k,i} (C_{k,i}^o - C_k^o) + \frac{1}{N} \sum_{i=1}^N \epsilon_{k,i}^2 \quad (12)$$

The second term on the left side of equation (12) is a sum of the product of two independent random values, and can be neglected which produces

$$\overline{c_k c_k} = (1 + \tau_k)^2 \overline{c_k^o c_k^o} + \epsilon_k^2 \quad (13)$$

Here, ϵ_k is the RMS value of the random error $\epsilon_{k,i}$. The bias error for the normal stress can then be determined as

$$\beta_{c_k c_k} = \overline{c_k c_k} - \overline{c_k^o c_k^o} = \overline{c_k c_k} - \frac{\overline{c_k c_k} + \epsilon_k^2}{(1 + \tau_k)^2} \approx \frac{2\tau_k \overline{c_k c_k} + \epsilon_k^2}{(1 + \tau_k)^2} \quad (14)$$

The bias error of the shear stress can also be derived in the same way as

$$\beta_{c_m c_n} = \left[1 - \frac{1}{(1 + \tau_m) \cdot (1 + \tau_n)} \right] \overline{c_m c_n} \approx \frac{(\tau_m + \tau_n) \overline{c_m c_n}}{(1 + \tau_m) \cdot (1 + \tau_n)} \quad (15)$$

The bias limits of the Reynolds stresses resulting from the PIV data reduction can be determined as

$$B_{kk} = \left| \frac{2\tau_k^* \overline{c_k c_k} + \epsilon_k^2}{(1 + \tau_k^*)^2} \right| \quad (16)$$

$$B_{mn} = \left| \frac{(\tau_m^* + \tau_n^*) \overline{c_m c_n}}{(1 + \tau_m^*) \cdot (1 + \tau_n^*)} \right| \quad (17)$$

where τ_k^* ($k=1, 2, 3$) is the limit of the bias gradient of the mean velocity component. When the bias sources of the coordinate deviations are included, the bias limits of the Reynolds stresses are finally determined by

$$B_{c_m c_n}^2 = B_{mn}^2 + (\theta_x^{mn} B_x)^2 + (\theta_y^{mn} B_y)^2 + (\theta_z^{mn} B_z)^2, \quad (16)$$

where $m=n=k$ for the normal stress and $m \neq n$ for the shear stresses. The sensitivity coefficients for the coordinate deviation are

$$\theta_x^{mn} = \frac{\partial \overline{c_m c_n}}{\partial x}, \quad \theta_y^{mn} = \frac{\partial \overline{c_m c_n}}{\partial y}, \quad \theta_z^{mn} = \frac{\partial \overline{c_m c_n}}{\partial z}, \quad (17)$$

for $m=1, 2, 3$ and $n=1, 2, 3$.

4.3

Precision limits

For a single test, the precision limit of a measured variable X is given by

$$P_X = K \cdot S_X \quad (18)$$

where K is the coverage factor and equals 2 for a 95% confidence level, S_X is the standard deviation of the sample of M readings of the variable X and is defined as

$$S_X = \sqrt{\frac{1}{M-1} \sum_{k=1}^M [X_k - \bar{X}]^2} \quad (19)$$

and the mean value is defined as

$$\bar{X} = \frac{1}{M} \sum_{k=1}^M X_k \quad (20)$$

In the present study, a single realization of X is defined as the statistical analysis of 1200 vector maps. The precision limits are determined with equation (18) after 8-10 repeated measurements for xy ($z=-0.03$) and xz ($y=-0.0425$) configurations at regions of high and low turbulence in the nominal wake.

4.4

Total uncertainty

The total uncertainty for the measured variables U_X is defined as the RSS of the bias and precision limits

$$U_X = \sqrt{B_X^2 + P_X^2} \quad (21)$$

5

Results

The mean velocities measured by PIV are shown in Figure 1 in comparison with those measured by 5-hole pitot probe (Longo and Stern 1999). Figure 1a and 1b are the contours of U and crossplane vectors VW , respectively. PIV data for U shows a pattern of relatively thin boundary layer near the centerplane and waterplane, but with a large thick boundary layer region (bulge) near midgirth and towards the centerplane. The bulge is likely due to the interaction of the sonar dome wake vortices and hull boundary layer. VW is upwards and toward the centerplane. The distributions of the Reynolds stress contours are given in Figure 2a-e. The patterns are similar to the U contours. The peak levels of turbulence are near the keel and towards the centerplane except for \overline{uv} which has peak levels near the center of the bulge.

Comparisons between the PIV and 5-hole pitot probe measurements demonstrate good agreement, both qualitatively and quantitatively, between the two measurement systems. The boundary layer bulge (U) is broader along the z -coordinate for the 5-hole pitot probe data. For VW , the magnitudes are generally smaller for the PIV data in the area outside the region of peak turbulence. Where the turbulence is highest, VW agree very well between measurement systems. The direction of VW agree very well everywhere throughout the measurement area.

Categorization of the bias error sources and contributions to the bias limit for U are provided as an example in Table 1 and are somewhat representative of all the measured results. The biases are either estimated from calibrations (L_{obj} , L_{img} , x , y , z), listed from manufacturer's specifications (Δt), taken from historical data (U_c), or computed with simulations and real tests (S_k). Combining the bias sources and sensitivity coefficients reveals the contributions of each source to B_U and focus points for reducing B_U . For instance, the primary bias error source is the evaluation bias, which can be reduced by further improvement of the evaluation algorithm. In addition, the scale factor (L_{obj}/L_{img}) uncertainty can be improved with a more refined calibration. In Table 2, the bias limit magnitudes B_X and contributions to U_X for each result is listed. Note that for the mean flow, the bias limit contribution is fairly high except for U , which is less than 50%. For the Reynolds stress results, the level of bias limit contribution to U_X is consistently and relatively low, i.e., <40%. Efforts to improve U_X for the mean flow should focus on reducing the bias error sources.

The precision limit magnitudes and contributions to U_X for each variable is listed in Table 2. The trends above in all variables for contributions of B_X to U_X are reversed for the

precision limits, i.e., most notably, contributions of P_X to U_X for the Reynolds stresses are greater than for B_X . The precision limits can be reduced by increasing the number of measurement samples for the statistical analysis.

The uncertainties of the PIV mean velocity components, expressed as percentages of the dynamic range (D_X) of the variables, are 2.4, 7.7, and 4.4% for U , V , and W , respectively. U_V and U_W appear large because D_X is 0-20% of U_c for these variables. The uncertainty in the Reynolds stresses is 4~6% of the respective dynamic ranges and is considered very good in comparison to previous estimates for LDV data uncertainties.

The average comparison error throughout the measurement area between the two measurement systems is 2.0, 11.8, and 9.7% for U , V , and W , respectively. Although the 5-hole pitot probe uncertainties (Table 2) for U , V , W are smaller than for the PIV uncertainties, one cannot conclude that the PIV uncertainties are outside the noise of the 5-hole pitot probe system due to unresolved bias error issues of the 5-hole pitot probe in a shear flow. More testing and analysis is required for a conclusive evaluation of the 5-hole pitot probe data quality.

6

Conclusions

A towed PIV system designed by DANTEC Measurement Technology for the Iowa Institute of Hydraulic Research towing tank is commissioned by measuring the mean velocity and Reynolds stresses at the nominal-wake plane of a model-scale ship. The mean velocities are compared with previous 5-hole pitot probe data. Uncertainty assessment following standard procedures is used to quantify the comparisons and reach conclusions regarding the quality of the data.

The PIV results of mean velocity components are qualitatively and quantitatively similar to 5-hole pitot probe measurements. The largest differences are in regions of high velocity gradient and turbulence where biases are likely for the 5-hole pitot probe, which are not accounted for in usual calibration procedures. The uncertainty of the PIV measurements can further be reduced by improving the evaluation algorithm of the image maps and by increasing the number of measurement samples.

Currently, unsteady tests are underway with DTMB model 5512 and a new plunger-type wavemaker in the IIHR towing tank. The PIV system will be used to measure the unsteady flow field of the model in regular head waves.

Acknowledgements

This research was sponsored by the Office of Naval Research under Grant N000 14-96-0018 administered by Dr. E.P. Rood.

References

- AIAA Standard, (1995), Assessment of Wind Tunnel Data Uncertainty, AIAA S-071-1995, Washington D.C.
- Coleman, H.W. and Steele, W.G., (1995), "Engineering Application of Experimental Uncertainty Analysis," AIAA Journal, Vol. 33, No. 10, pp. 1888-1896.

Dong, R.R., Katz, J., and Huang, T.T., (1997), “On the structure of bow waves on a ship model,” *J. Fluid Mechanics*, Vol. 346, pp. 77-115.

Dring, R.P., (1982), “Sizing criteria for laser anemometry particles,” *J. Fluids Engineering*, Vol. 104, pp. 15-17.

Longo, J., Huang, H.P., Stern, F., (1998), “Solid/free-surface juncture boundary layer and wake,” *Exp. Fluids*, Vol. 25, pp. 283-297.

Gui, L., Longo, J., Stern, F., (1999), “Biases of PIV measurement of turbulent flow and the masked correlation-based interrogation algorithm,” *Exp. Fluids*, (in preparation).

Longo, J. and Stern, F., (1996), “Yaw effects on model-scale ship flows,” *Proceedings of the 21st ONR Symposium on Naval Hydrodynamics*, Trondheim, Norway, pp. 312-327.

Longo, J. and Stern, F., (1999), “Resistance, sinkage and trim, wave profile, and nominal wake tests and uncertainty assessment for DTMB model 5512,” 25th ATTC, Iowa City, IA., (in publication).

Stern, F., Longo, J., Maksoud, M., and Suzuki, T., (1998), “Evaluation of Surface-Ship Resistance and Propulsion Model-Scale Database for CFD Validation,” 1st Symposium on Marine Applications of Computational Fluid Dynamics, McLean, VA.

Toda, Y., Stern, F., and Longo, J., (1992), “Mean-Flow Measurements in the Boundary Layer and Wake and Wave Field of a Series 60 C_B=0.60 Ship Model - Part 1: Froude Numbers 0.16 and 0.316,” *Journal of Ship Research*, Vol. 36, No. 4, pp. 360-377.

Westerweel, J., (1997), “Fundamentals of digital particle image velocimetry,” *Meas. Sci. Technology*, Vol. 8, pp. 1379-1393.

Table 1: Bias limits of the mean axial velocity (U) component

Variable X	Unit	Magnitude	B _x	θ _x	B _x θ _x	%
L _{obj}	m	0.0747	0.00025	12.1078	3.0269×10 ⁻³	24.32%
L _{img}	pixel	1008	0.5	-8.9727×10 ⁻⁴	0.4486×10 ⁻³	3.60%
Δt	second	0.0049	0.0000001	-1.8458×10 ⁻³	0.1846×10 ⁻³	1.48%
U _c	m/s	1.53	0.003561	-0.5911	2.1051×10 ⁻³	16.91%
S	pixel	9.1498	0.05	0.0988	4.9425×10 ⁻³	39.70%
x	—	—	0.5/3048	-0.1596	0.0262×10 ⁻³	0.21%
y	—	—	0.5/3048	2.1234	0.3483×10 ⁻³	2.80%
z	—	—	0.5/3048	-8.3304	1.3665×10 ⁻³	10.98%
U	—	0.9044	6.3440×10 ⁻³	—	—	—

Table 2: Summary of the PIV and 5-hole pitot probe uncertainty assessment results

Variable X	D _x	B _x	%	P _x	%	U _x	%	
PIV (all values nondimensional)								
U	[10 ⁻²]	45.883	0.6344	42.05%	0.8742	57.95%	1.0801	2.35%
V	[10 ⁻²]	6.8495	0.4949	72.35%	0.1891	27.64%	0.5298	7.73%
W	[10 ⁻²]	13.409	0.5021	62.38%	0.3028	37.62%	0.5863	4.37%
\overline{uu}	[10 ⁻³]	3.0518	0.0365	20.77%	0.1392	79.23%	0.1439	4.72%
\overline{vv}	[10 ⁻³]	1.4489	0.0295	34.88%	0.0551	65.12%	0.0625	4.31%
\overline{ww}	[10 ⁻³]	1.3090	0.0334	37.26%	0.0562	62.74%	0.0654	4.99%
\overline{uv}	[10 ⁻³]	1.0319	0.0062	13.03%	0.0417	86.97%	0.0422	4.09%
\overline{uw}	[10 ⁻³]	1.0586	0.0243	30.10%	0.0564	69.90%	0.0614	5.80%
5-hole pitot probe (all values nondimensional)								
U	[10 ⁻²]	61.600	0.7922	88.34%	0.2878	11.66%	0.8429	0.84%
V	[10 ⁻²]	13.300	0.1538	58.60%	0.1292	41.40%	0.2009	1.51%
W	[10 ⁻²]	15.500	0.1824	86.05%	0.0735	13.95%	0.1967	1.10%

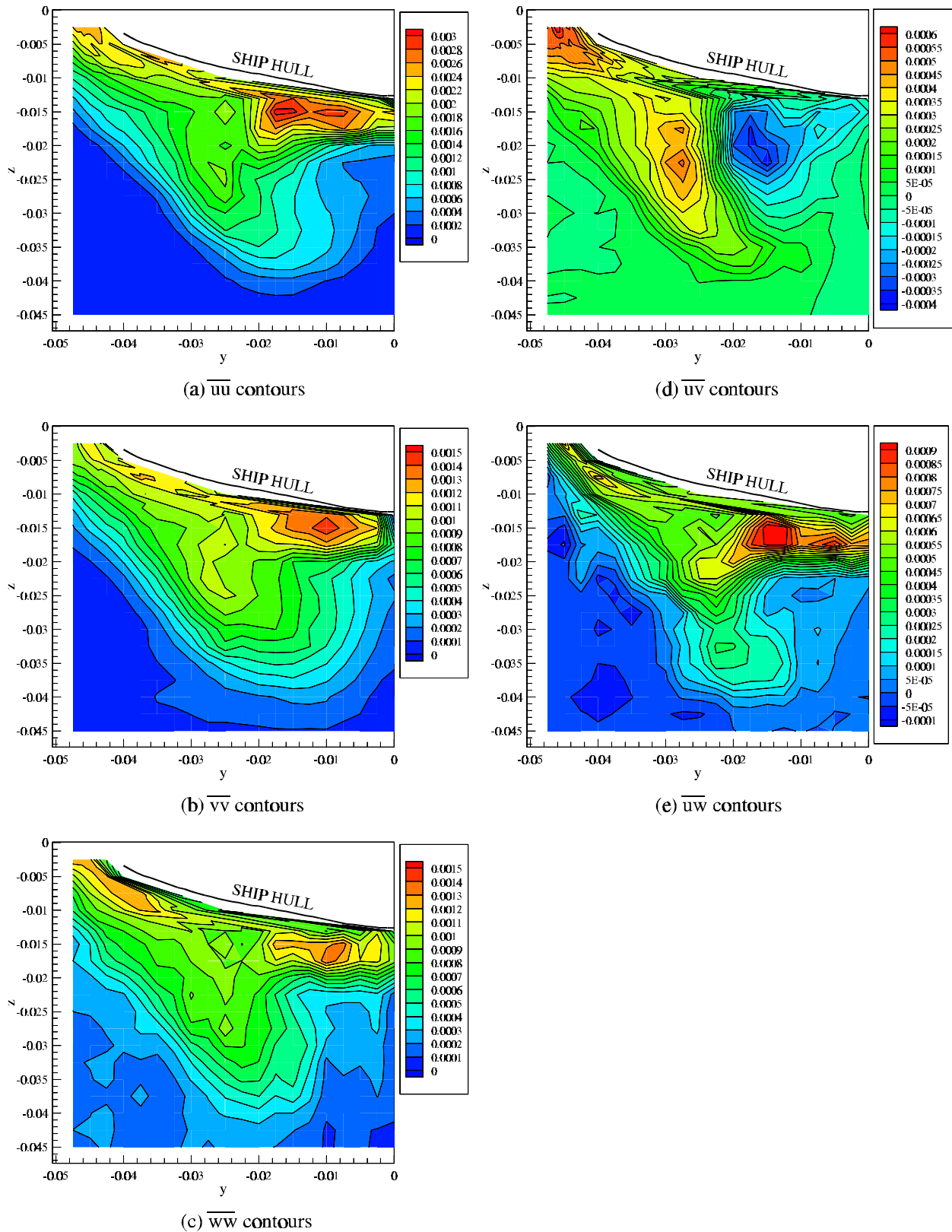


Fig. 2 Reynolds stresses measured by PIV in the nominal-wake plane of DTMB model 5512: $L=3.048$, $x=0.935$, $U_c=1.53$ m/s ($Fr=0.28$)